PAPER

Injectable hydrogels of optimized acellular nerve for injection in the injured spinal cord

Biomedical Materials

PAPER

Injectable hydrogels of optimized acellular nerve for injection in the injured spinal cord

RECEIVED
19 August 2017

REVISED
15 December 2017

ACCEPTED FOR PUBLICATION
30 January 2018

PUBLISHED
21 March 2018

R Chase Cornelison[1,2], Elisa J Gonzalez-Rothi[3], Stacy L Porvasnik[2], Steven M Wellman[2], James H Park[2], David D Fuller[3] and Christine E Schmidt[2]

[1] McKetta Department of Chemical Engineering, University of Texas at Austin, Austin, TX 78712, United States of America
[2] J. Crayton Pruitt Family Department of Biomedical Engineering, University of Florida, Gainesville, FL 32611, United States of America
[3] Department of Physical Therapy, University of Florida, Gainesville, FL 32611, United States of America

E-mail: schmidt@bme.ufl.edu

Keywords: acellular nerve graft, extracellular matrix, *in situ* gelling, hydrogel, neural tissue engineering, spinal cord injury

Supplementary material for this article is available online

Abstract

Objective. Spinal cord injury (SCI) affects a quarter million individuals in the United States, and there is currently no clinical treatment. Both fresh and acellular peripheral nerve grafts can induce spinal axon regeneration and support functional recovery in experimental injury models. Nonetheless, a scaffold that can be injected into a spinal contusion would be far less invasive to apply. We aimed to develop the first injectable acellular nerve graft for promoting repair after contusion SCI. *Approach*. We report a method to enzymatically solubilize optimized acellular (OA) nerve—a decellularized peripheral nerve graft developed in our laboratory and currently used clinically—to obtain an injectable solution that undergoes thermal gelation under physiological conditions. We quantified multiple physical and compositional properties of this novel material as well as tested its efficacy at acute and chronic time points following cervical contusion SCI. *Main Results*. This injectable optimized acellular (iOA) nerve graft retains native chemical cues such as collagens and glycosaminoglycans. By varying hydrogel concentration, the rheological properties and compressive modulus of iOA were similar to that previous reported for rat central nervous tissue. iOA solution was compatible with rat Schwann cells in culture, and hydrogel injection into a rat cervical contusion model significantly reduced the ratio of M1:M2 macrophages after one week, favoring regenerative phenotypes ($p < 0.05$). Furthermore, while iOA treatment did not affect locomotor or respiratory recovery over an eight week period, the percentage of axonal coverage increased at the distal tissue interface ($p < 0.05$), suggesting enhanced axonal extension within this region. *Significance*. Our data indicate that this novel injectable form of acellular nerve grafts is amenable for use after contusion SCI and may bolster a simultaneous therapy by acutely modulating the inflammatory milieu and supporting axonal growth.

1. Introduction

Damage to the spinal cord results in partial or complete paralysis below the injury level (NSCISC 2016). There is currently no treatment, rendering the ensuing deficits permanent. With nearly 60% of all injuries occurring at the cervical level, these deficits can be extremely debilitating, ranging from loss of locomotor function to respiratory dysfunction. In an effort to develop new therapies, contusion-type spinal cord injury (SCI) models have been established in animals which exhibit similar pathology to human injury, including cavitation and degeneration of the spinal cord (Gensel *et al* 2006). Regenerating damaged axons across this cavity to restore neurological function has proven challenging. Nonetheless, several experimental strategies have been developed in attempt to overcome regenerative limitations, including implanting growth-supportive scaffolds (Tom *et al* 2009, Patel *et al* 2010, Alilain *et al* 2011, Kanno *et al* 2014).

Unlike the central nervous system, the peripheral nervous system has an inherent, albeit limited,

capacity for regeneration. This dichotomy is often attributed to differences between matrix composition and supportive glial cell populations (Gonzalez-Perez *et al* 2013, Lutz and Barres 2014). Researchers have been grafting segments of peripheral nerve into the spinal cord for decades to capitalize on this divergent regenerative ability (David and Aguayo 1981, Tom *et al* 2009, Alilain *et al* 2011). Although fresh nerve grafts show particular promise to promote tissue regeneration and functional recovery, this strategy often requires sustained immunosuppression to mitigate the immunogenicity of fresh tissue allografts (though not autografts). Decellularization provides a means to overcome the possibility of immune rejection without requiring tissue harvest from the patient (Carriel *et al* 2014). Acellular nerve grafts are in fact now used clinically for peripheral nerve repair, including one product based on research from our lab (Hudson *et al* 2004, Daly *et al* 2011, Carriel *et al* 2014). Researchers have recently begun using acellular nerve grafts experimentally in the spinal cord with moderate success, suggesting acellular nerve grafts may have translational potential in this area, as well (Chu *et al* 2012, Li *et al* 2012). Nonetheless, implanting an intact graft into the spinal cord may require undesirable excision of healthy tissue for optimal integration.

Injectable formulations of acellular tissue are a growing trend in tissue engineering. Such materials have been used experimentally to repair a variety of tissues, including cardiac muscle, skeletal muscle, cartilage, bone, and peripheral nerve (Freytes *et al* 2008, Seif-Naraghi *et al* 2010, DeQuach] *et al* 2011, 2012, Medberry *et al* 2013, Prest *et al* 2017). Based on the clinical success of acellular nerve grafts and experimental benefits of nerve grafts in the spinal cord, an injectable acellular nerve graft may offer an effective and clinically translatable scaffold for spinal cord regeneration. Furthermore, it has been shown that injectable, ECM-mimicking matrices increase the efficacy of cellular therapies for SCI, such as Schwann cell transplantation (Patel *et al* 2010). Because many cell therapies, including Schwann cell therapy, are under investigation in clinical trials, developing a clinically-relevant, injectable scaffold to enhance these therapeutic outcomes would be of great clinical significance. An injectable acellular nerve graft may be optimally suited for this task by capitalizing on the regenerative potential of nerve ECM. Further, emerging research suggests that acellular tissues can enhance pro-regenerative immune responses after injury, increasing the therapeutic potential of such therapies (Brown *et al* 2012, Sicari *et al* 2014, Ghuman *et al* 2016).

The objectives of this work were to develop and characterize a novel injectable scaffold derived from optimized acellular nerve scaffold (iOA) suited for minimally-invasive injection following contusion SCI. We examined (1) the composition and mechanics compared to native nerve and spinal tissue, respectively, (2) cell survival *in vitro* and acute macrophage response *in vivo*, and (3) functional and tissue regeneration following implantation into a rat model of cervical contusion SCI. Collectively, these analyses revealed that iOA nerve hydrogels have potential to promote neural repair and may be an effective platform for combination SCI therapy.

2. Materials and methods

2.1. Nerve decellularization and digestion

Sciatic nerves were aseptically harvested from adult Sprague Dawley rats, separated from the epineurium, and decellularized according to Hudson *et al* (2004). All processing was performed in sterile conditions at room temperature on a vertical agitator set to 14 rpm. Nerve tissue was subjected to alternating solutions of 125 mM sulfobetaine-10 and 0.14% Triton X-200/0.6 mM SB-16. The tissue was washed with a 100 mM sodium/50 mM phosphate buffered solution between detergent changes with three final rinses in a 50/10 mM sodium phosphate solution. To remove potentially inhibitory chondroitin sulfate proteoglycans, the acellular nerves were then treated with 200 μl 0.02 U ml^{-1} chondroitinase ABC (Sigma) for 16 h at 37 °C (Neubauer *et al* 2007). The tissue was washed three times in 1X phosphate buffered saline (PBS) for 3 h, three times in sterile ddH_2O for 15 min, flash frozen, lyophilized for 48 h (Labconco FreeZone4.5), and stored at −20 °C.

A protocol to solubilize OA nerve and achieve thermal gelation was developed based on previous literature for other tissues (Freytes *et al* 2008, DeQuach *et al* 2011). Briefly, dried acellular nerve tissue was weighed and cut into 1–2 mm segments using microscissors. The tissue pieces were then added to a solution of 1 mg ml^{-1} porcine pepsin (Sigma) and 0.01 M HCl at a concentration of 20 mg ECM ml^{-1}. The digestion was conducted at room temperature under constant stirring for 60–64 h. After complete digestion, the enzyme was deactivated by raising the pH to 7.4 using sterile 1 M NaOH (1/100th original volume) and sterile 10X PBS (to 1X final dilution). The resulting nerve solution was diluted to desired concentrations using 1X PBS for *in vitro* material characterization or *in vivo* implantation, as described below.

2.2. Collagen and glycosaminoglycan quantification

The collagen and sulfated glycosaminoglycan (sGAG) contents of acellular nerve were determined using Sircol and Blyscan assay kits (Biocolor Ltd, UK), respectively, performed according to manufacturer's instructions (Medberry *et al* 2013, Roosens *et al* 2016). For the collagen assay, nerve tissue was digested at 20 mg ml^{-1} in 1 mg ml^{-1} pepsin for 64 h at room temperature, and for the sGAG assay, tissue was digested at 20 mg ml^{-1} in a solution of 0.1 mg ml^{-1} papain (Sigma) (containing 0.2 M monobasic sodium phosphate, 0.1 M sodium acetate, 5 μM EDTA, and

5 μM cysteine) for 18 h at 65 °C. sGAG content was measured both before and after chondroitinase ABC treatment to distinguish residual heparin/keratin sulfates from chondroitin/dermatan sulfate proteoglycans. All data were normalized to the dry weight of the tissue and are represented in units of mg mg^{-1} ($n = 11$ in duplicate for collagen content, and $n = 5$ in duplicate for sGAG content). Additionally, tissues from age- and sex-matched animals were also normalized to tissue length to account for mass changes during decellularization that may skew the results. These data are represented in units of μg mm^{-1} ($n = 5$ in duplicate for both assays).

2.3. Turbidity gelation kinetics

The gelation kinetics of injectable nerve solution was assessed by incubating 100 μl of cold nerve solution in each well of an ice-cold 96-well plate. The plate was immediately transferred from ice to a Biotek Synergy HT spectrophotometer preheated to 37 °C. Absorbance at 405 nm was measured every 2 min for 30 min to detect protein aggregation or crosslinking. Normalized absorbance was calculated according to equation 1 (Medberry *et al* 2013) and used to determine the lag time of gelation, t_{lag}; the slope of gelation, s; and the time to achieve 50% and 95% maximum absorbance, $t_{1/2}$ and t_{95}, respectively. The analysis was repeated three times in duplicate.

$$\text{Normalized absorbance} = \frac{A - A_0}{A_{max} - A_0}. \quad (1)$$

2.4. Scanning electron microscopy

iOA hydrogels at 16.5 mg ml^{-1} were fixed in 4% paraformaldehyde for 30 min at room temperature, washed in ddH_2O, and dehydrated onto glass slides by incubating for 15 min each in (v/v) aqueous solutions of 30%, 50%, 70%, 85%, 90%, 95%, and 100% ethanol and 30 min each in ethanol solutions of 25%, 50%, 75%, 100% hexamethyldisilazane (Sigma) (Fozdar *et al* 2011). The samples were left to dry overnight in a fume hood. For comparison, 10 μm thick longitudinal sections of fresh nerve were fixed in 4% paraformaldehyde for 10 min and similarly dehydrated. Conductive tape (Electron Microscopy Sciences) was applied to establish an electrical connection between the metal chuck and the dehydrated hydrogel sample. Mounted samples were then sputter coated with 10 nm of Au/Pd and imaged on a field emission gun scanning electron microscope (FEI).

2.5. Mechanical characterization

Compressive and shear testing were performed to examine the mechanical properties of nerve hydrogels for comparison to native rat neural tissue. Nerve hydrogels at 16.5, 13, and 9.5 mg ml^{-1} were molded to a defined geometry using 8 mm cylindrical silicon molds (Grace Biolabs) by incubation at 37 °C for 15 min. The compressive modulus of the hydrogels at each concentration was measured using an Instron 5542 (Instron Corp). Samples were compressed at a rate of 0.1 mm s^{-1} until 60% extension (Seidlits *et al* 2010). The slope of the linear region (within the first 20% of strain) for the resulting stress–stain curve was calculated and represents the compressive modulus. Additionally, the viscoelastic properties were examined using an Anton Paar MCR 302 rheometer with parallel plate geometry according to established methods (Johnson *et al* 2011, Zuidema *et al* 2014). A sandblasted, 8 mm top load cell was used to decrease slipping during testing. To approximate physiological conditions, the Peltier plate was pre-heated to 37 °C, and the samples were enclosed in a humidity chamber. Amplitude sweeps from 0.01% to 100% were first conducted at 6 rad s^{-1} to determine the linear viscoelastic (LVE) range. The storage (G') and loss (G'') moduli were then determined using frequency sweeps from 0.1 to 100 Hz at a strain value in the middle of the LVE, chosen as 0.5% strain for all concentrations.

2.6. *In vitro* schwann cell culture and live/dead assessment

Etched glass coverslips were coated either with a 20 μg ml^{-1} solution of poly-D-lysine (PDL; Fisher) overnight at room temperature or 1 mg ml^{-1} iOA for 1 h at 37 °C. Neonatal rat Schwann cells (passage 2–3; Sciencell) were plated onto coated coverslips at 30 000 cells per coverslip (approximately 27 000 cells cm^{-2}), allowed to adhere for 20 min at 37 °C, and incubated in 3:1 DMEM:F12 medium containing 1% penicillin-streptomycin (Fisher), 2% N2 neural supplement (Invitrogen), 5 μM forskolin (Sigma), and 50 ng ml^{-1} neuregulin (R&D Systems). After 3 days, a live/dead assay was performed according to manufacturer's instructions (Invitrogen). Fluorescence images were obtained at 10X magnification using an Olympus IX70 with DP80 dual color digital camera and CellSens software. The numbers of total cells and dead cells were counted using the 'Analyze Particles' function in ImageJ (NIH). For total cell counts, individual cells were discriminated using the standard ImageJ 'watershed' function in binary mode prior to analysis. Cell numbers were averaged for three frames in each sample ($n = 5$, repeated three times).

2.7. Cervical contusion SCI and hydrogel injection

The initial immune response to nerve hydrogel implantation was assessed using a clinically-relevant model of unilateral, cervical contusion SCI in adult rats. All procedures involving animals were approved by the Institutional Animal Care and Use Committee at the University of Florida. Briefly, Sprague Dawley rats (250–300 g, Charles River) were anesthetized using isoflurane. The spinal cord was exposed using a laminectomy at the third and fourth cervical vertebrae (C3/4). A unilateral contusion between C3 and C4 was created using an infinite horizon impactor equipped

with a 2.5 mm impactor tip at a set force of 200 kDynes (Sandrow-Feinberg *et al* 2009, Tom *et al* 2009). Only contusions from impact forces that were within 10% of the desired force (200 ± 20 kDy) were included in the study. Approximately 80% of contusion injuries fell within this criteria, necessitating a 20% overestimation of group numbers (e.g., starting with eight animals per group to obtain a final six per group). The muscle layers and skin were closed using 5–0 resorbable Vicryl and monofilament nylon sutures, respectively. Buprenorphine (0.03 mg kg^{-1}; Patterson Veterinary) was administered subcutaneously for forty-eight hours for pain management. Animals were monitored for excessive deficits and the ability to access food and water, provided ad libitum.

This model of SCI was found to yield a lesion volume of 6.16 ± 0.18 μl (average ± SEM; $n = 5$) one week after injury based on H&E staining (data not shown). Therefore, for all studies performed herein, 6 μl of either 1X PBS or iOA solution was injected into the lesion one week after injury at 1 μl per minute. The injection system included a 34 gauge needle on a Nanofil syringe mounted to an UltraMicroPump3 microinjection system (World Precision Instruments). Following injection, the needle was left in place for 2 min, then slowly retracted to prevent overflow from the lesion. Six animals were included in each injection group. Administration of buprenorphine was repeated and supplemented with meloxicam (1 mg kg^{-1}; Norbrook). Gentamicin (4 mg kg^{-1}; Patterson Veterinary) was also given subcutaneously for five days starting the day prior to injection to minimize the risk of infection. At study completion (two weeks post-injury for macrophage quantification and nine weeks, for regeneration assessment), animals were transcardially perfused with 1X PBS and 4% paraformaldehyde. Spinal columns were isolated and post-fixed in paraformaldehyde overnight before being transferred to 30% sucrose for cryopreservation.

2.8. Locomotor behavioral tests

Asymmetry in paw use was examined using the cylinder paw preference test (Khaing *et al* 2012). Animals were placed in a Plexiglass cylinder 20 cm in diameter, and forelimb use was scored during vertical exploration. The first forelimb to contact the wall was scored as independent use of that limb, receiving either a 'left' or 'right' score. If the opposite limb was then placed on the wall, no score was given until the first limb was moved, requiring independent use of the second limb for support. A score of 'both' was given if both forepaws contacted the wall simultaneously. Alternation in limb use to climb the wall was also scored as 'both' for each set of forelimb movements. To score again, both forepaws had to be removed from the wall. Only paw placements in the ascending or lateral directions were scored for a total of 20 scores. The percent of ipsilesional paw use was calculated by adding the percentage of ipsilesional placements and half the percentage of 'both' placements. The forelimb locomotor score (FLS) was used to examine voluntary forelimb recovery during open field locomotion (Cao *et al* 2008). As detailed in supplemental table 1 is available online at stacks.iop.org/BMM/13/034110/mmedia, FLS is an 18-point rating system (0–17) where 0 indicates no function and 17, normal function. This test assesses forelimb use during locomotion based on joint movement, the ability to bear weight on the affected limb, and the ability to achieve clearance during stepping. Two blinded investigators performed the test by placing individual rats or pairs of rats on a textured, round table top for four minutes each (six minutes for pairs), scoring independent use of both forelimbs. Testing was performed weekly, starting the week prior to injury as a baseline for comparison. Animals were enticed to follow a pencil or piece of paper if there were hesitant to walk across the open field.

2.9. Phrenic nerve recordings

Nerve recording procedures were conducted at 8 weeks post-transplantation as adapted from previous literature (Doperalski *et al* 2008, Fuller *et al* 2008, Fuller *et al* 2009). Urethane anesthetized animals (1.6 g kg^{-1}) received a tracheal cannulation (PE-240 tubing) to enable mechanical ventilation, and tracheal pressure was continuously monitored (DTXPlus Pressure Transducer, Argon Critical Care Systems, Singapore; Model TA-100 strain gauge amplifier, CWE Inc.). Both vagus nerves were sectioned to prevent phrenic motor entrainment with the ventilator rate. A femoral artery catheter was used to measure blood pressure (DTXPlus Pressure Transducer, Argon Critical Care Systems, Singapore; Model TA-100 strain gauge amplifier, CWE Inc.) and withdraw blood samples. Arterial PO_2 (PaO_2) and PCO_2 ($PaCO_2$) and pH were determined using an i-Stat blood gas analyzer (Heska), and end-tidal CO_2 partial pressure ($PETCO_2$) was measured throughout the experiment (Capnogard, Novametrix Medical Systems). A neuromuscular paralytic was given to eliminate spontaneous breathing efforts (pancuronium bromide, 2.5 mg kg^{-1}, i.v., Hospira, Inc.). Blood pressure and fluid homeostasis were maintained by i.v. infusion of a 1:3 solution of sodium bicarbonate (8.4%) and Lactated Ringers.

Phrenic nerve output was recorded using bipolar silver wire suction electrodes filled with 0.9% saline. Signals were amplified (x10 000) and band-pass filtered (3–30 000 Hz) using a differential A/C amplifier, digitized (CED Power 1401 data acquisition interface) and integrated in real time (time constant = 20 ms) using Spike2 software (Cambridge Electronic Design Limited, Cambridge, England). The end-tidal CO_2 apneic threshold for inspiratory activity was determined by gradually decreasing the inspired CO_2 until inspiratory phrenic bursting ceased. After 2–3 min

inspired CO_2 was gradually increased until inspiratory bursting resumed. For the remainder of data collection, the $PETCO_2$ was maintained at 2 mmHg above the value at which bursting resumed. An arterial blood sample was drawn following a 10 min baseline (inspired $O_2 = 50\%$). Rats were then exposed to 5 min of hypoxia (11% O_2). Following a 10 min recovery period, rats were exposed to a 5 min bout of hypercapnia (50% O_2; 9% CO_2). Following another 10 min recovery period, the mechanical ventilator was briefly stopped (~10 s) to produce a maximal chemoreceptor stimulus. The already deeply anesthetized rats were then euthanized via systemic perfusion.

2.10. Immunohistochemistry and digital image analysis

Cryopreserved spinal cords were prepared for cryosectioning as stated above. All antibody information is summarized in supplemental table 2. At one week, the tissue was assessed for total macrophage infiltration and macrophage polarization toward either an M1, pro-inflammatory phenotype or an M2, pro-regenerative phenotype Additionally, axons were labeled using mouse anti-neurofilament 200 kD (NF) and glial scarring was identified using rabbit anti-glial fibrillary acidic protein (GFAP, Abcam). At the eight week time point, the tissue was stained with chicken anti-neurofilament (Aves Labs) to label axons, rabbit anti-glial fibrillary acidic protein (GFAP, Abcam) to identify glial scarring, and mouse anti-CD68 (Abd Serotec) to label macrophages/microglia. Briefly, tissue sections were incubated with blocking buffer containing 3% goat serum and 0.3% Triton X100 for 1 h at room temperature. Primary antibodies were then added in blocking buffer and incubated overnight at 4 °C. Samples were washed 3 × 10 min with 1X PBS, and secondary antibodies in blocking buffer were added for 1 h in the dark at room temperature. The PBS washes were repeated, and DAPI was added (1:1000 in water) for 5 min in the dark to label cell nuclei. Stained samples were then mounted using Fluoromount-G (SouthernBiotech) and coverslipped for imaging. Images were obtained using a Zeiss Axio Imager.Z2 and Zen software. Immune cell number was quantified using Zen image analysis software. Each marker was assessed in the lesion epicenter in six sections approximately 120 μm apart.

2.11. Statistics

One-way analysis of variance on GraphPad Prism software followed by Tukey's test was used to identify statistical differences within multiple groups (glycosaminoglycan analysis and rheological measurements). For data having only two groups (collagen assessment, cytocompatibility studies, histological quantification, and functional assessments), a student's t-test was used to determine significance. Grubbs' test was used to identify any significant outliers ($p < 0.05$), resulting in exclusion of one technical replicate (of six) for each experimental group for the one week immune cell quantification. All error bars are represented as standard error of the mean, unless otherwise stated.

3. Results

3.1. Pepsin solubilization of acellular nerve enables thermal gelation under physiological conditions

Nerve tissue was decellularized according to our previously developed method (Hudson *et al* 2004) and used to create an injectable nerve hydrogel. The digestion parameters found to be optimal for converting decellularized nerve tissue into a thermally gelling hydrogel are as follows: lyophilized nerve was cut into ~1 mm segments, added to 1 mg ml^{-1} pepsin at a concentration of 20 mg ECM ml^{-1}, and digested at room temperature with constant stirring for 60–64 h, similar to prior reports (Freytes *et al* 2008, DeQuach *et al* 2012, DeQuach *et al* 2011). After quenching digestion, the nerve pre-gel solution rapidly formed a hydrogel when placed at 37 °C in a humidified chamber (figure 1). Gelation kinetics were examined by measuring solution turbidity over 30 min at concentrations of 16.5, 13, and 9.5 mg ml^{-1}, and observed gelation parameters are summarized in table 1. Unsurprisingly, less concentrated solutions were slower to initiate gelation, with lag times of 4.9, 5.8, and 6.5 min for 16.5, 13, and 9.5 mg ml^{-1}, respectively. Nonetheless, all solutions achieved 95% gelation within 10–11 min. This time frame is sufficiently long enough to enable easy handling during injection yet rapid enough to enable efficient encapsulation of cells for transplantation *in vivo*. The resulting hydrogels were fibrous in structure, as observed using scanning electron microscopy (figure 1(B)). The hydrogels contained fiber diameters on the same length scale as those in native nerve tissue, approximately 100 nm (figure 1(C)). These fibers were also similar in size to those in collagen I hydrogels (not shown), suggesting collagen I fibrillogenesis contributes to the thermal gelation properties of iOA hydrogels under physiological conditions.

We examined the rheological properties of iOA hydrogels at different concentrations, as well as the compressive modulus at the highest concentration. The storage and loss moduli were found to decrease with decreasing concentration (table 2). At 16.5 mg ml^{-1}, iOA hydrogels exhibited a storage modulus of 171 ± 8.3 Pa and a loss modulus of 25.2 ± 1.65 Pa. Hydrogels made at 13 and 9.5 mg ml^{-1} had lower storage moduli, approximately 70.5 ± 5.44 and 31.3 ± 1.44 Pa, respectively. Because the storage modulus at 16.5 mg ml^{-1} was similar to rodent and human neural tissue (Levental *et al* 2007), we also evaluated the compressive modulus and found it to be approximately 4.51 ± 0.354 kPa (table 2). Adult rat brain has been previously reported by our lab at around 5 kPa (Seidlits *et al* 2010).

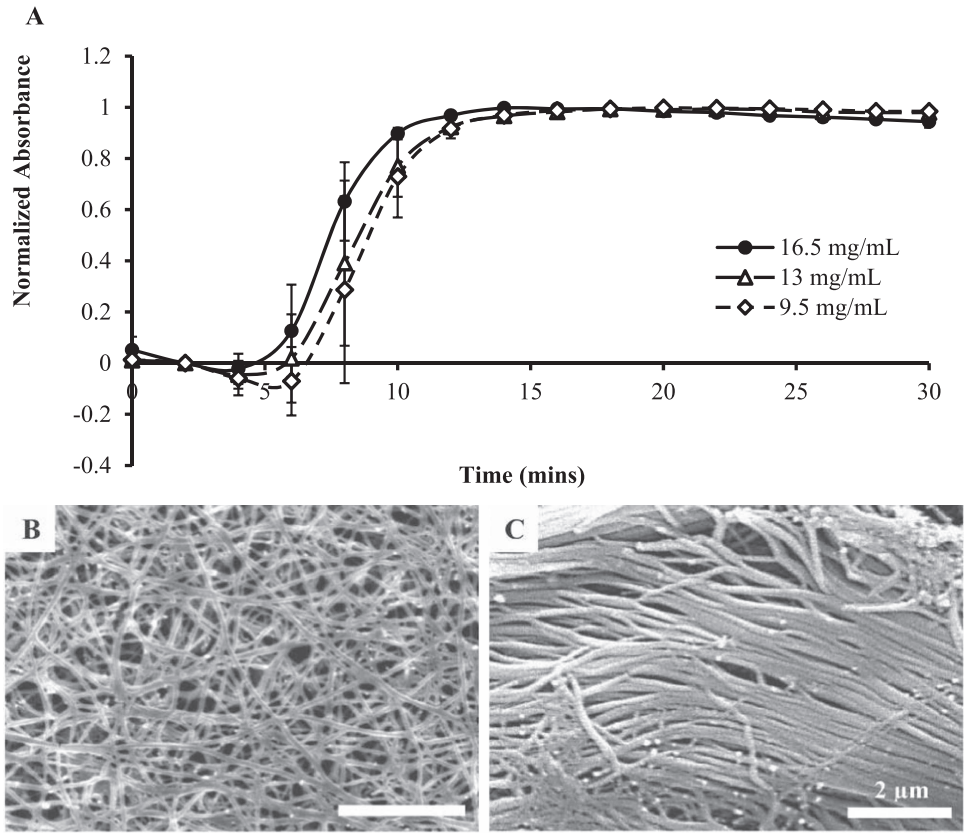

Figure 1. iOA gels rapidly at 37 °C, forming a fibrous structure reminiscent of native nerve tissue. (A) iOA solutions at 16.5 mg ml^{-1} initiated gelation faster than those at lower concentrations, but all solutions achieved gelation in 11–12 min. (B) The hydrogel structure was assessed using scanning electron microscopy. Fibers on the order of 80–100 nm were visible in iOA hydrogels following gelation. These fibers were of similar dimensions as those found in native peripheral nerve (C).

Table 1. Calculated gelation kinetic parameters for iOA at 37 °C. Lag time, t_{lag}, is the time from $t = 0$ until the region of linear increase; $t_{1/2}$ and t_{95} are the times to achieve 50% and 95% gelation, respectively; s is the speed of gelation calculated as the slope of the linear region.

	Reported value (mean ± SEM)		
Parameter	16.5 mg ml^{-1}	13 mg ml^{-1}	9.5 mg ml^{-1}
t_{lag} (mins)	4.88 ± 1.25	5.82 ± 1.24	6.46 ± 1.05
$t_{1/2}$ (mins)	7.50 ± 0.61	8.30 ± 0.87	8.70 ± 0.86
t_{95} (mins)	10.0 ± 0.19	10.9 ± 0.87	11.2 ± 1.18
s (mins)$^{-1}$	0.19 ± 0.04	0.18 ± 0.01	0.20 ± 0.01

3.2. Hydrogels of iOA nerve retain factors of native neural tissue

We found that collagen content increased after decellularization when normalizing to tissue weight (figure 2(A)), from 8.90% ± 0.938% in fresh nerve to 23.7% ± 2.19% in iOA nerve ($n = 11$, $p < 0.0001$). To enable comparison independent of mass (which changes as a result of decellularization), we also normalized to tissue length for age and sex matched animals. Normalized to length, total collagen decreased from 27.2 ± 4.64 µg mm^{-1} to 15.3 ± 3.27 µg mm^{-1} for fresh and iOA nerve, respectively, though this difference was not significant (figure 2(B)) ($n = 5$; $p = 0.07$). Performing similar analyses for GAG content, iOA contained 1.79 ± 0.108 µg mg^{-1} or 86.9 ± 2.88 ng mm^{-1} compared to 0.884 ± 0.033 µg mg^{-1} or 252 ± 11.4 ng mm^{-1} in fresh tissue, respectively (figures 2(C) and (D)) ($n = 5$; $p < 0.01$ and $p < 0.001$). Additionally, we used chondroitinase ABC to selectively remove chondroitin/dermatan sulfate proteoglycans because this was previously suggested to increase regenerative into nerve grafts (Neubauer *et al* 2007). The treated acellular nerve tissue retained 39.8 ± 3.07 ng mm^{-1} or approximately 16% of the original GAG content. For more characterization of decellularized, intact nerve, refer to Hudson *et al* (2004).

3.3. iOA hydrogels support cell survival *in vitro* and interact with inflammation *in vivo*

Prior to *in vivo* injection, iOA nerve solution was examined to support cell attachment and survival *in vitro*. Because Schwann cells are native to peripheral nerve, this cell type was used as a 'best case' model for examining cell survival. Rat Schwann cells were plated on 2D glass coverslips coated either with PDL or iOA, and cell attachment and survival was assessed after 3 days in culture. A live/dead assay revealed no significant difference in cell survival on the two substrates, with over 95% survival on both coatings (figure 3(A)). Additionally, cell attachment was the same for the control and nerve substrates at 750 ± 31 and 775 ± 25 cells/frame, respectively (figure 3(B)).

Table 2. Summary data for mechanical characterization. Storage (G'), loss (G''), and compressive moduli are shown for each tested hydrogel concentration, when applicable. All data are in Pascals and reported as mean ± standard error.

Concentration	G'	G''	Compressive modulus
16.5 mg ml^{-1}	170.9 ± 3.31	25.2 ± 1.65	4517.7 ± 354.6
13 mg ml^{-1}	70.5 ± 5.44	21.88 ± 2.03	—
9.5 mg ml^{-1}	31.3 ± 1.44	9.47 ± 0.36	—

We also explored the immune-modifying potential of iOA by injecting one week after injury and evaluating macrophage phenotypes after an additional week. Immunofluorescence staining for the pan-macrophage marker CD68 revealed an extensive macrophage/microglia presence inside the lesion and occasionally on the uninjured side (not shown). A portion of these cells could be identified as M1 cells by CCR7 staining (figures 4(A) and (B)) while others were found to express markers of M2 cells such as CD206 (figures 4(C) and (D)). Using digital image analysis, it was found that the number of CCR7$^+$ macrophages was relatively unchanged by treatment, but the number of CD206$^+$ macrophages dramatically increased following iOA injection. This effect significantly shifted the ratio of M1 to M2 macrophages from 1.88 ± 0.406 for PBS controls to 0.635 ± 0.085 for iOA (figure 4(I); $p < 0.05$). No immediate effect was found on astrocytic scarring or neuronal sparing (supplemental figure 1).

3.4. Nerve hydrogels increase axonal growth to the distal tissue interface at 8 weeks post-injection

To examine if iOA nerve hydrogels can support long-term spinal cord regeneration, a second cohort of animals was carried out to 8 weeks post-implantation to examine locomotor functional recovery, respiratory recovery, and histological outcomes for axon regeneration, glial scarring, and immune response. The extent of neural regeneration was first assessed using immunohistochemistry. Longitudinal tissue sections were used to evaluate the cellular level response to PBS and injectable nerve injection after cervical contusion SCI. Eight weeks after injection, both groups exhibited axonal staining in the lesion epicenter. The staining was mostly punctate in animals treated with PBS (figures 5(A)–(C)), but fine fiber projections could be found in the lesion and at the distal interface between the lesion and intact tissue for animals treated with injectable nerve (figures 5(D)–(F)). Quantification of axonal staining was consistent with these observations. In contrast to the lesion epicenter, where no statistical difference in axonal coverage was observed (figure 5(G)), iOA treatment significantly increased axonal staining in adjacent distal (healthy) tissue (figure 5(H)). No effects were observed on astrocytic scarring (figure 5(I)), total macrophage staining (not shown) or total volume of spared tissue based on Luxol Fast Blue staining (supplemental figure 2).

3.5. iOA hydrogels do not hinder functional recovery from cervical SCI

Forelimb function was longitudinally assessed for 8 weeks after injection using three behavior tests: cylinder paw preference, forelimb locomotor scale, and vibrissae-elicited paw placing. No significant differences were observed between the PBS and iOA experimental groups for either test. At 8 weeks post-injection (9 weeks post-injury), animals treated with iOA and PBS used their injured paw for vertical exploration in 8.5% and 6.6%, of attempts, respectively (figure 6(A)). Both groups received FLS scores between 12–13 out of 17 for the ipsilateral paw, indicating continuous plantar support of the injured paw during walking with either rotated (12) or parallel (13) paw placement on stepping (figure 6(B)). The contralateral paw did not demonstrate any functional deficits and was consistently scored at 17.

Respiratory function was quantified by recording electrical activity of both phrenic nerves in mechanically ventilated, vagatomized rats (Lee *et al* 2013). Data were recorded during baseline conditions and respiratory challenges with brief exposure to reduced O_2 (hypoxia) or elevated CO_2 (hypercapnia). In addition, a maximum response was evoked at the end of the recording session by briefly stopping the mechanical ventilator to trigger a combined hypoxic-hypercapnic stimulus. Representative phrenic nerve activity and arterial blood pressure recorded for one PBS-treated and one injectable nerve-treated animal are show in supplemental figure 3. In figure 6, ipsilateral phrenic amplitude is presented as the absolute value of the electrical signal (i.e., raw data in mV) (C) and (D) and also normalized to the contralateral phrenic nerve discharge (E) or the discharge during baseline conditions (F). No differences were observed between the experimental averages for any measure or normalization method. Importantly, these careful respiratory neurophysiological assays confirm that the injectable hydrogels do not impair respiratory recovery.

4. Discussion

Promoting repair of the injured spinal cord remains a difficult task. The lesion that develops following SCI lacks a growth-supportive substrate, limiting axonal regrowth and tissue healing. *In situ* forming hydrogels are ideal for supplanting this lost matrix as they can be applied without damage to the surrounding, uninjured

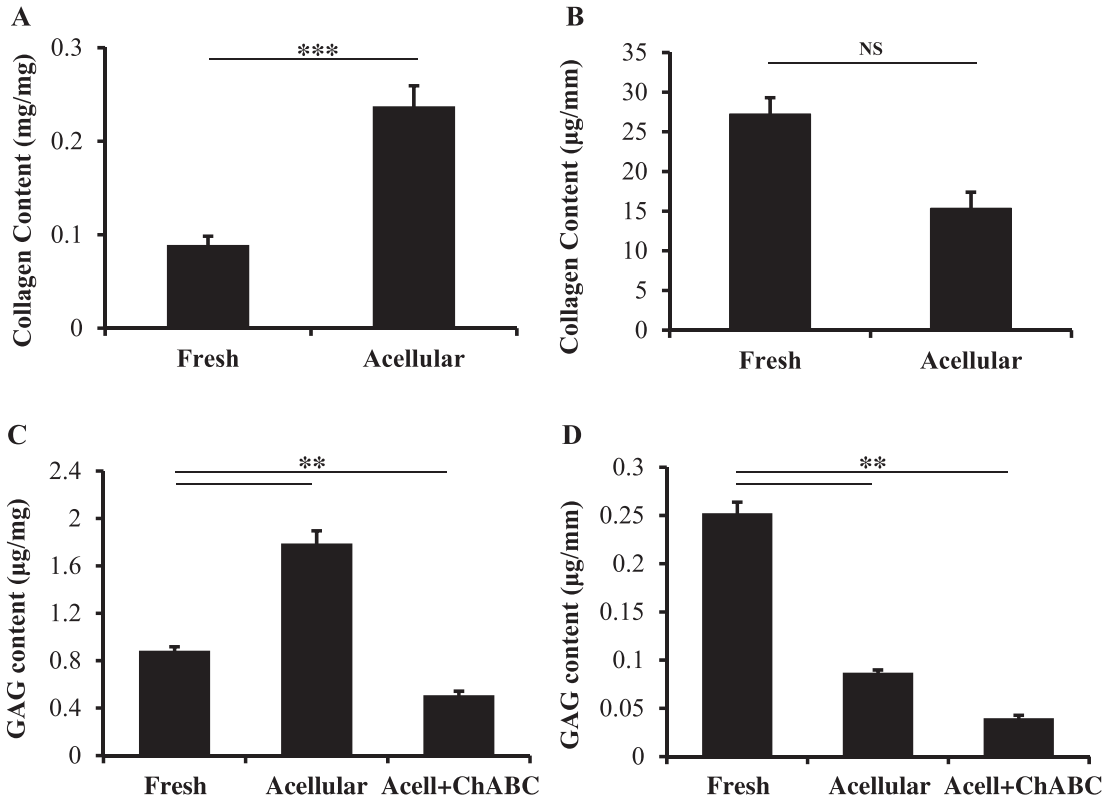

Figure 2. Biochemical characterization of optimized acellular nerve. (A), (B) Collagen content of acellular nerve. (A) Collagen content significantly increased after decellularization when normalized to mass ($p < 0.0001$; $n = 11$). (B) Normalizing to length showed only a slight, but insignificant, decrease after decellularization ($p = 0.069$; $n = 5$). (C), (D) Sulfated glycosaminoglycan (sGAG) content. (C) As with collagen, mass normalization showed an increase in sGAGs after decellularization ($n = 5$). (D) Normalizing to tissue length showed 66% reduction in sGAG content ($n = 5$). After treating with chondroitinase ABC to remove inhibitory chondroitin sulfate proteoglycans, acellular nerve retained 15% of the original sGAGs. ** and *** indicate $p < 0.01$ and $p < 0.001$, respectively. NS = not significant, $p = 0.07$. Error bars represent standard error.

tissue. Further, *in situ*-forming materials directly integrate with host tissue to enhance astrocyte/axon interactions (Williams *et al* 2015). There are several recent efforts to develop injectable matrices from decellularized tissues to treat a variety of injuries (Freytes *et al* 2008, DeQuach *et al* 2011, 2012, Seif-Naraghi *et al* 2012). While most studies have sourced extracellular matrix from the same tissue as that of the injury site, injectable urinary bladder matrix has now been applied into both the brain and spinal cord following stroke and SCI, respectively (Ghuman *et al* 2016, Tukmachev *et al* 2016). These studies showed modest benefits, but it may be important to consider that neural-specific matrices (i.e., derived from neural tissue) can enhance neurite outgrowth and neural cell differentiation compared to non-neural tissue sources (Freytes *et al* 2008, Kigerl *et al* 2009).

Tukmachev *et al* (2016) observed enhanced axonal staining coverage using injectable acellular spinal cord compared to urinary bladder at 8 weeks, though the effects were not significant. For decades, grafts of peripheral nerve have shown promise for promoting regeneration of injured spinal axons (David and Aguayo 1981, Tom *et al* 2009, Alilain *et al* 2011, Sachdeva *et al* 2016). Acellular peripheral nerve has more recently been shown to be similarly supportive (Tajdaran *et al* 2016). We propose that an injectable acellular peripheral nerve graft may be well-suited to promote repair following SCI. Our lab previously developed an optimized decellularization protocol specific for peripheral nerve (Hudson *et al* 2004). Here, we report building on this technology via enzymatic digestion of optimized acellular (OA) nerve grafts to create an injectable OA nerve hydrogel for use following contusion SCI.

Decellularized nerve was effectively solubilized using pepsin digestion to achieve a solution which rapidly gelled at physiological conditions. This injectable OA hydrogel (iOA) was fully gelled by 11 min for all three concentrations tested (16.5, 13, 9.5 mg ml^{-1}). Gelation was likely caused by collagen fibrillogenesis given that fibers on the same length scale as those in native nerve and collagen I were observed in the hydrogel structure. Additionally, iOA nerve retained 56% of the original collagen content of fresh nerve tissue. A portion of the original sulfated GAG content also remained, which may help increase growth factor binding/bioactivity (Colin *et al* 1999, Jiao *et al* 2007) and enhance *in vivo* outcomes (Hill *et al* 2012, Seif-Naraghi *et al* 2012).

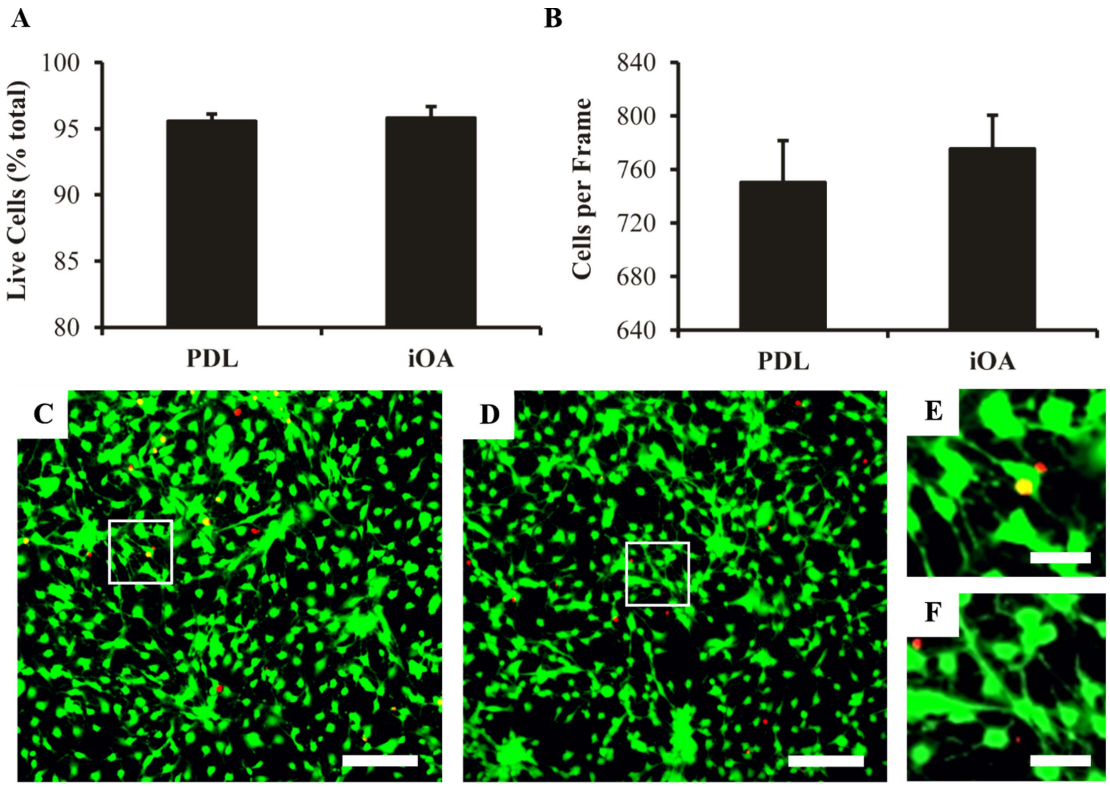

Figure 3. iOA nerve solution supports cell survival and attachment comparable to controls. (A) Schwann cell survival and (B) cell adherence on coated glass coverslips after 3 days *in vitro* ($n = 3$). Representative 10X images for survival quantification are shown for PDL (C) and iOA (D), with live cells in green and dead cells in red. Magnified inset images are shown in (E) and (F), respectively. No difference was observed between PDL controls and iOA coated coverslips ($p = 0.75$). $n = 6$ per group. Scale bars are 200 μm, and error bars represent standard error.

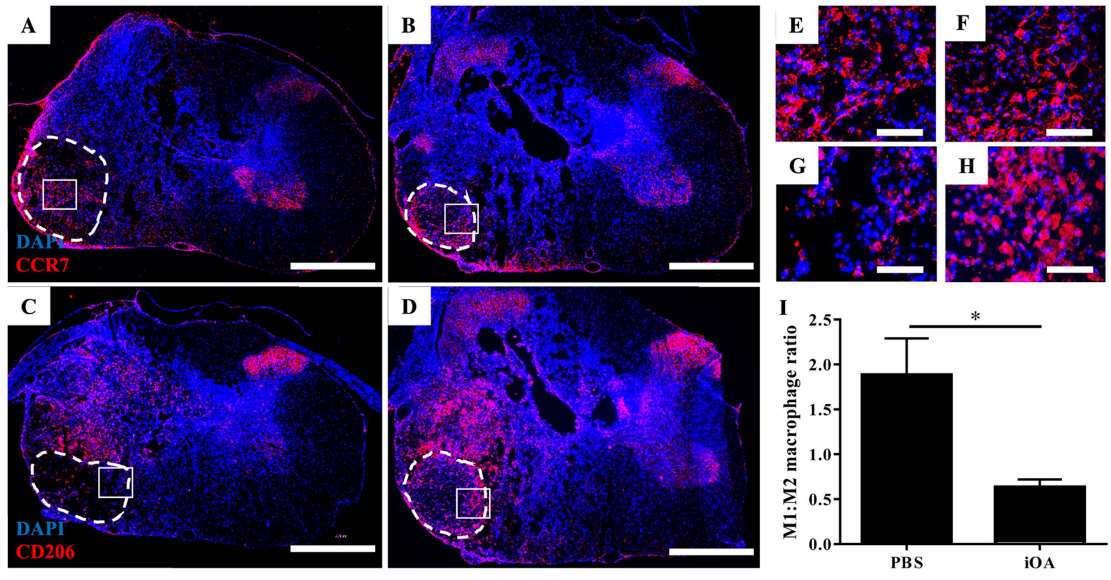

Figure 4. Injection of iOA hydrogels in the injured spinal cord can influence macrophage phenotype. Animals were treated with PBS (A) and (C) or iOA hydrogels (B) and (D) for one week, and spinal cord cross-sections were stained for macrophage markers. (A)–(C) Fluorescence micrographs show representative staining for CCR7 for M1 macrophages (red; (A) and (B)) and CD206 for M2 macrophages (red; (C) and (D)). Nuclei are counterstained with DAPI (blue). (E)–(H) Indicated inset images of (A)–(D), respectively, better depict criteria for positive staining. Scale bars are 200 μm (A)–(D) and 50 μm (E)–(H). (I) The number of M1 and M2 macrophages was digitally quantified for CCR7 and CD206 stained sections. A three-fold reduction in the M1:M2 ratio was observed for iOA injection compared to PBS controls ($^{*}p < 0.05$; $n = 4$).

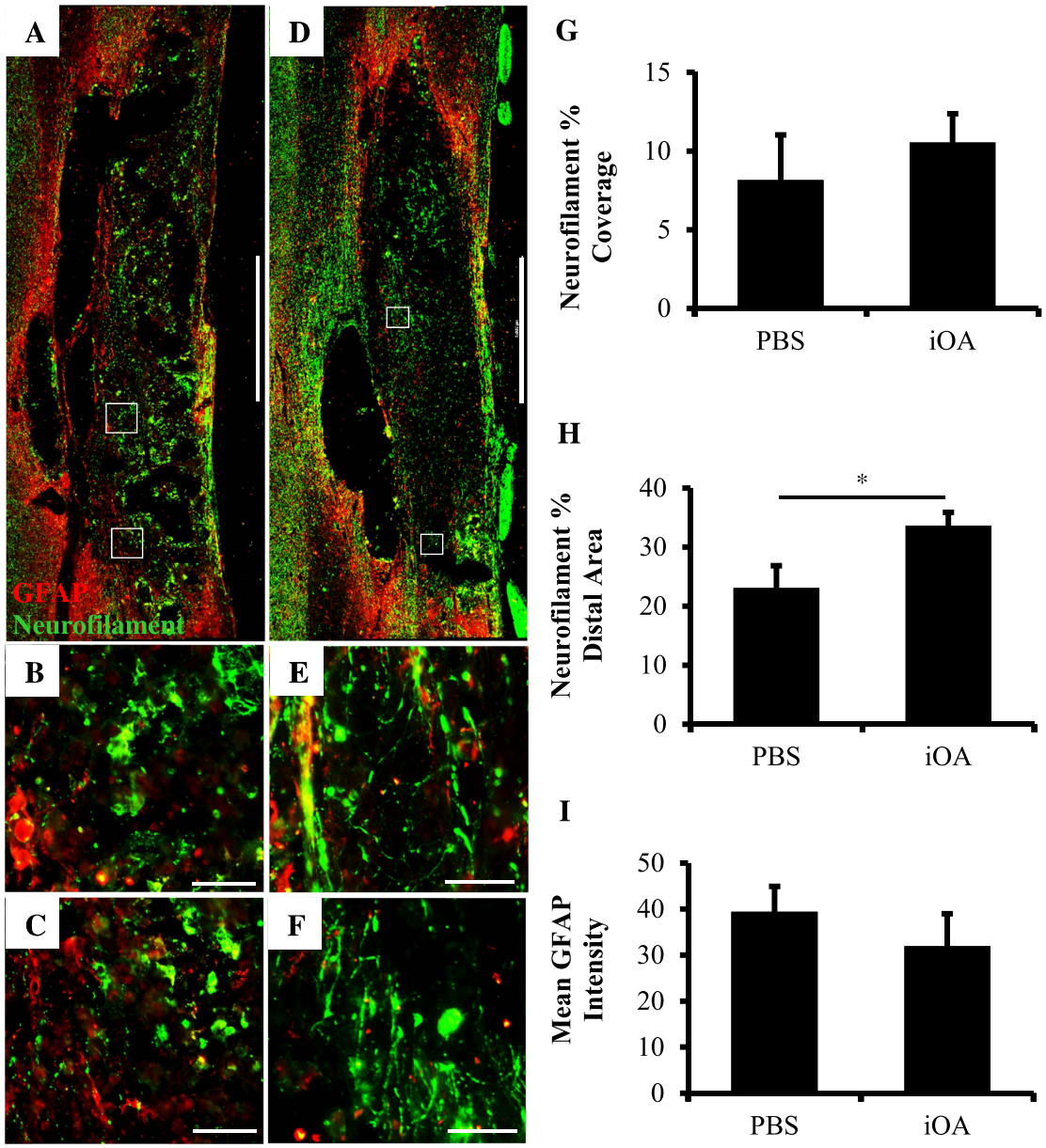

Figure 5. More axonal projections are observed in the lesion and entering the distal interface after injectable nerve treatment. (A)–(F) Fluorescence images of longitudinal sections stained for glial scarring (GFAP, red) and axons (neurofilament, green). Representative images for animals treated with PBS are shown in (A)–(C) and those treated with iOA hydrogels in (D)–(F). Inset images (B), (C) and (E), (F) correspond to (A) and (D), respectively. Scale bars are 1000 μm (A) and (D) and 50 μm (B), (C), (E), and (F). (G) Quantification of neurofilament coverage in the lesion. (H) Quantification of neurofilament coverage at the distal interface. (I) Mean GFAP intensity of the glial scar tissue around the lesion. $^{*}p < 0.05; n = 7$.

We examined the mechanical properties of iOA hydrogels by looking at the response to both shear and compressive forces. Because hydrogel concentration can influence deliverability and *in situ* gelling ability (Massensini *et al* 2015), we again examined the properties at three concentrations. The mechanical properties were shown to be adjustable by simply changing the hydrogel concentration, with storage and loss moduli decreasing in proportion to concentration. iOA hydrogels at 16.5 mg ml^{-1} exhibited a storage modulus of 171 ± 8.3 Pa (table 2). This value is similar to reports for rat brain and human gray matter, each with a modulus of approximately 200 Pa (Levental *et al* 2007). Hydrogels made at 13 and 9.5 mg ml^{-1} exhibited lower storage moduli, approximately 70.5 ± 5.44 and 31.3 ± 1.44 Pa, respectively. The compressive modulus for 16.5 mg ml^{-1} hydrogels was approximately 4.51 ± 0.354 kPa (table 2), in range of adult rat brain (Seidlits *et al* 2010) and that previously reported optimal for promoting neurite growth in 3D cell culture (Man *et al* 2011).

The macrophage response to a biomaterial is a commonly used parameter for evaluating the response to implantation, as assessed by the ratio of pro-inflammatory M1 macrophages to anti-inflammatory M2 macrophages (Brown *et al* 2009, Mokarram *et al* 2012, Sicari *et al* 2014, Kelly *et al* 2017, Wang *et al* 2017). The spinal cord is initially occupied primarily by M2 macrophages

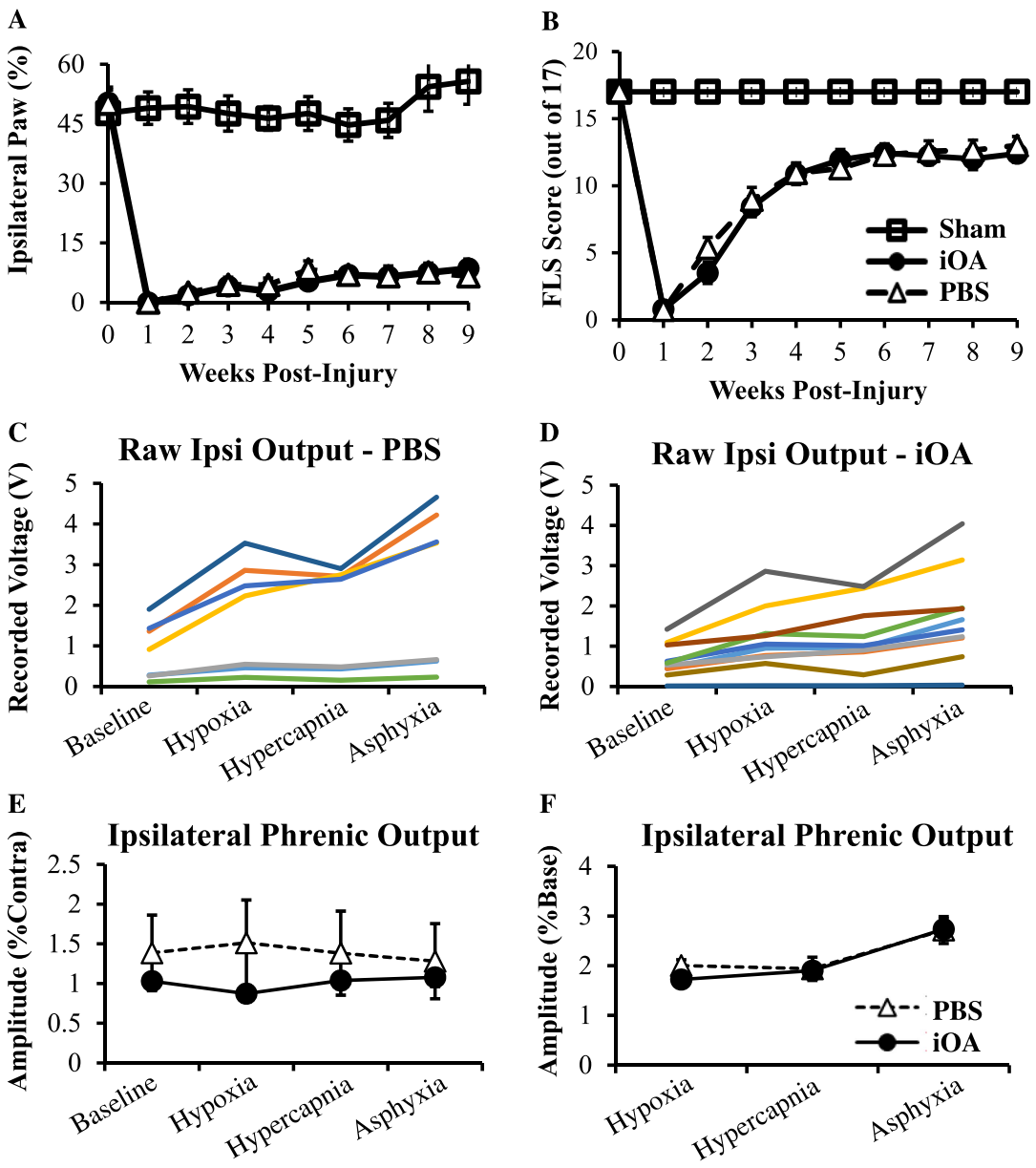

Figure 6. Injectable nerve was not detrimental to recovery after SCI. Forelimb function was examined over 8 weeks using (A) cylinder paw preference and (B) forelimb locomotor scale behavioral assessments. No significant difference was observed between the two groups for either test ($n = 13$). (C)–(F) Recordings from bilateral phrenic nerves were taken 8 weeks post-injection. Neural output was recorded under baseline conditions (50% O_2), hypoxia (11% O_2), hypercapnia (50% O_2 7% CO_2), and asphyxia (ventilator disabled). (C), (D) Raw amplitude data for ipsilateral nerves of each animal. PBS-treated animals ($n = 7$) displayed a bimodal distribution while iOA-treated animals ($n = 8$) showed a more distributed response. Ipsilateral phrenic amplitude was averaged for each group and normalized to (E) contralateral output or (F) baseline response. No difference was observed between treatments for either normalization ($n = 7$).

which transition toward M1 phenotypes around two weeks following injury (Kigerl *et al* 2009). Recent work demonstrated that implanting injectable acellular tissue increased M2 gene signatures after stroke (Ghuman *et al* 2016). Therefore, we explored the immune-modifying potential of iOA one week after injection. For this study, as with the later regenerative study, we employed a clinically-relevant unilateral cervical contusion model and injected the material one week after injury. iOA injection caused a significant decrease in the ratio of M1 to M2 macrophage phenotypes, shifting from primarily pro-inflammatory (M1:M2 > 1) to primarily anti-inflammatory (M1:M2 < 1). This change could have significant implications for increasing survival of any transplanted cells as well as limiting deleterious effects on tissue degeneration/regeneration. Nonetheless, it should be noted that co-staining of these markers, and certainly use of additional markers, would provide a more thorough analysis of the effects of iOA on macrophage phenotype.

This reduction in the ratio of macrophage phenotypes at an acute timepoint unfortunately did not

confer benefits to functional recovery over an 8 week period. Separate forelimb functional tests and phrenic neurograms demonstrated that iOA did not support, but also did not hinder, recovery. We did, however, observe an increase in axonal coverage at the distal entrance site. These results potentially indicate the presence of iOA hydrogels assisted in axonal reentry into healthy tissue, albeit without increasing function. Total macrophage coverage was also unaffected; yet, because much of the $CD68^{+}$ staining appeared diffuse and reminiscent of cellular debris, it was difficult to quantify macrophage phentoypes in the manner used one week after injection. Taken together, our data indicate that iOA nerve hydrogels (1) can be applied in a minimally-invasive fashion, (2) gel *in situ* to form a supportive scaffold with mechanical properties comparable to neural tissue, and (3) offer some potential to favor repair processes following contusion SCI, but may require combination with other interventions for significant functional and tissue recovery.

The rate of material degradation may explain why injectable nerve alone did not demonstrate observable functional benefits. The enzymatic pre-treatment of acellular tissue required to create an injectable tissue graft essentially pre-degrades the ECM such that the material residence time may be substantially decreased. And because the onset of axon regeneration is typically 4–6 weeks post injury, materials to promote spinal cord regeneration may require longer residence times than those found to promote functional recovery in other injury paradigms. At one week post-implant, the iOA material was distinguishable within the lesion by collagen staining (supplemental figure 4); however, the material was not observable after 8 weeks, suggesting the material had degraded and/or been remodeled. A similar study recently drew similar conclusions (Tukmachev *et al* 2016). Collagen matrices are widely studied for their ability to support axon extension and neural regeneration (Deister *et al* 2007, Patel *et al* 2010, Myers *et al* 2011); therefore, the absence of such a matrix could effectively slow or prevent recovery. Injectable tissue grafts for treating SCI may require the addition of exogenous cells that can produce their own extracellular matrix as the original delivery vehicle degrades. This combination approach would not only increase the initial survival or viability of transplanted cells but could also indirectly provide a newly deposited matrix to support axonal ingrowth and functional recovery. Alternatively or concurrently, drug or gene delivery could be used to further enhance regeneration (Dumont *et al* 2016, Führmann *et al* 2017).

5. Conclusions

The list of potential applications for decellularized tissues in tissue engineering and regenerative medicine continues to grow, particularly following the advent of *in situ* forming scaffolds (Freytes *et al* 2008). Acellular nerve grafts are currently only used to repair peripheral nerve defects in the clinic, but an injectable version would enable translation of this promising therapeutic material for SCI repair, as well. We created a less invasive, injectable scaffold of acellular nerve for treating contusion SCI or other forms of neural injury by building on a decellularization technology developed in our lab and now used clinically for peripheral nerve applications. This injectable acellular nerve graft (iOA) approximated the chemical, mechanical, and topographical properties of native peripheral nerve upon thermal gelation under physiological conditions. We showed that iOA hydrogels decreased the ratio of M1:M2 macrophages in the sub-acute SCI environment compared to saline controls, an indication of bias toward a regenerative, anti-inflammatory phenotype. While no long-term functional benefit or deficit was observed after iOA injection, the percentage of axonal coverage in the distal spinal cord was increased in treated animals after 8 weeks. This iOA nerve hydrogel therefore shows potential as a minimally-invasive scaffold for treating contusion SCI and may prove useful for enhancing the therapeutic benefit of other deliverable factors.

Acknowledgments

We would like to thank Dr Peter McFetridge for allowing us to use his Instron. This work was supported by the National Institute of Health: R21EB013358 (CES), R21NS074162 (CES), 1R01NS080180-01A1 (DDF); NIH/NINDS Research Supplement to Promote Diversity (NS80180) (EGR); Craig Neilsen Foundation grant #222456 (CES); University of Florida's University Scholars Program (JHP); and a National Science Foundation travel award (RCC).

ORCID iDs

R Chase Cornelison https://orcid.org/0000-0002-0651-717X
Christine E Schmidt https://orcid.org/0000-0002-5865-6016

References

Alilain W J, Horn K P, Hu H, Dick T E and Silver J 2011 Functional regeneration of respiratory pathways after spinal cord injury *Nature* **475** 196–200

Brown B N, Ratner B D, Goodman S B, Amar S and Badylak S F 2012 Macrophage polarization: an opportunity for improved outcomes in biomaterials and regenerative medicine *Biomaterials* **33** 3792–802

Brown B N, Valentin J E, Stewart-Akers A M, McCabe G P and Badylak S F 2009 Macrophage phenotype and remodeling outcomes in response to biologic scaffolds with and without a cellular component *Biomaterials* **30** 1482–91

Cao Y, Shumsky J S, Sabol M A, Kushner R A, Strittmatter S, Hamers F P T, Lee D H S, Rabacchi S A and Murray M 2008 Nogo-66 receptor antagonist peptide (NEP1-40) administration promotes functional recovery and axonal

growth after lateral funiculus injury in the adult rat *Neurorehabil. Neural Repair* **22** 262–78
Carriel V, Alaminos M, Garzón I, Campos A and Cornelissen M 2014 Tissue engineering of the peripheral nervous system *Expert Rev. Neurother.* **14** 301–18
Chu T H, Wang L, Guo A, Chan V, Wong C and Wu W 2012 GDNF-treated acellular nerve graft promotes motoneuron axon regeneration after implantation into cervical root avulsed spinal cord *Neuropathology Appl. Neurobiol.* **38** 681–95
Colin S, Jeanny J C, Mascarelli F, Vienet R, Al-Mahmood S, Courtois Y and Labarre J 1999 *In vivo* involvement of heparan sulfate proteoglycan in the bioavailability, internalization, and catabolism of exogenous basic fibroblast growth factor *Mol. Pharmacol.* **55** 74–82
Daly W, Yao L, Zeugolis D, Windebank A and Pandit A 2011 A biomaterials approach to peripheral nerve regeneration: bridging the peripheral nerve gap and enhancing functional recovery *J. R. Soc. Interface* **9** 202–21
David S and Aguayo A J 1981 Axonal elongation into peripheral nervous system 'bridges' after central nervous system injury in adult rats *Science* **214** 931–3
Deister C, Aljabari S and Schmidt C E 2007 Effects of collagen 1, fibronectin, laminin and hyaluronic acid concentration in multi-component gels on neurite extension *J. Biomater. Sci. Polym. Ed.* **18** 983–97
DeQuach J A, Lin J E, Cam C, Hu D, Salvatore M A, Sheikh F and Christman K L 2012 Injectable skeletal muscle matrix hydrogel promotes neovascularization and muscle cell infiltration in a hindlimb ischemia model *Eur. Cells Mater.* **23** 400
DeQuach J A, Yuan S H, Goldstein L S and Christman K L 2011 Decellularized porcine brain matrix for cell culture and tissue engineering scaffolds *Tissue Eng.* A **17** 2583–92
Doperalski N J , Sandhu M S, Bavis R W, Reier P J and Fuller D D 2008 Ventilation and phrenic output following high cervical spinal hemisection in male vs female rats *Respir. Physiol. Neurobiol.* **162** 160–7
Dumont C M, Margul D J and Shea L D 2016 Tissue engineering approaches to modulate the inflammatory milieu following spinal cord injury *Cells Tissues Organs* **202** 52–66
Fozdar D Y, Lee J Y, Schmidt C E and Chen S 2011 Selective axonal growth of embryonic hippocampal neurons according to topographic features of various sizes and shapes *Int. J. Nanomed.* **6** 45–57
Freytes D O, Martin J, Velankar S S, Lee A S and Badylak S F 2008 Preparation and rheological characterization of a gel form of the porcine urinary bladder matrix *Biomaterials* **29** 1630–7
Führmann T, Anandakumaran P N and Shoichet M S 2017 Combinatorial therapies after spinal cord injury: how can biomaterials help? *Adv. Healthcare Mater.* **6** 1601130
Fuller D D, Doperalski N J, Dougherty B J, Sandhu M S, Bolser D C and Reier P J 2008 Modest spontaneous recovery of ventilation following chronic high cervical hemisection in rats *Exp. Neurol.* **211** 97–106
Fuller D D, Sandhu M S, Doperalski N J, Lane M A, White T E, Bishop M D and Reier P J 2009 Graded unilateral cervical spinal cord injury and respiratory motor recovery *Respir. Physiol. Neurobiol.* **165** 245–53
Gensel J C, Tovar C A, Hamers F P, Deibert R J, Beattie M S and Bresnahan J C 2006 Behavioral and histological characterization of unilateral cervical spinal cord contusion injury in rats *J. Neurotrauma* **23** 36–54
Ghuman H, Massensini A R, Donnelly J, Kim S M, Medberry C J, Badylak S F and Modo M 2016 ECM hydrogel for the treatment of stroke: characterization of the host cell infiltrate *Biomaterials* **91** 166–81
Gonzalez-Perez F, Udina E and Navarro X 2013 Extracellular matrix components in peripheral nerve regeneration *Int. Rev. Neurobiol.* **108** 257–75
Hill J J, Jin K, Mao X O, Xie L and Greenberg D A 2012 Intracerebral chondroitinase ABC and heparan sulfate proteoglycan glypican improve outcome from chronic stroke in rats *Proc. Natl Acad. Sci.* **109** 9155–60
Hudson T W, Liu S Y and Schmidt C E 2004 Engineering an improved acellular nerve graft via optimized chemical processing *Tissue Eng.* A **10** 1346–58
Jiao X, Billings P C, O'Connell M P, Kaplan F S, Shore E M and Glaser D L 2007 Heparan sulfate proteoglycans (HSPGs) modulate BMP2 osteogenic bioactivity in C2C12 cells *J. Biol. Chem.* **282** 1080–6
Johnson T D, Lin S Y and Christman K L 2011 Tailoring material properties of a nanofibrous extracellular matrix derived hydrogel *Nanotechnology* **22** 494015
Kanno H, Pressman Y, Moody A, Berg R, Muir E M, Rogers J H, Ozawa H, Itoi E, Pearse D D and Bunge M B 2014 Combination of engineered Schwann cell grafts to secrete neurotrophin and chondroitinase promotes axonal regeneration and locomotion after spinal cord injury *J. Neurosci.* **34** 1838–55
Kelly S H, Shores L S, Votaw N L and Collier J H 2017 Biomaterials strategies for generating therapeutic immune responses *Adv. Drug. Deliv. Rev.* **114** 3–18
Khaing Z Z, Geissler S A, Jiang S, Milman B D, Aguilar S V, Schmidt C E and Schallert T 2012 Assessing forelimb function after unilateral cervical spinal cord injury: novel forelimb tasks predict lesion severity and recovery *J. Neurotrauma* **29** 488–98
Kigerl K A, Gensel J C, Ankeny D P, Alexander J K, Donnelly D J and Popovich P G 2009 Identification of two distinct macrophage subsets with divergent effects causing either neurotoxicity or regeneration in the injured mouse spinal cord *J. Neurosci.* **29** 13435–44
Lee K Z, Dougherty B J, Sandhu M S, Lane M A, Reier P J and Fuller D D 2013 Phrenic motoneuron discharge patterns following chronic cervical spinal cord injury *Exp. Neurol.* **249** 20–32
Levental I, Georges P C and Janmey P A 2007 Soft biological materials and their impact on cell function *Soft Matter* **3** 299–306
Li C, Zhang X, Cao R, Yu B, Liang H, Zhou M, Li D, Wang Y and Liu E 2012 Allografts of the acellular sciatic nerve and brain-derived neurotrophic factor repair spinal cord injury in adult rats *PLoS One* **7** e42813
Lutz A B and Barres B A 2014 Contrasting the glial response to axon injury in the central and peripheral nervous systems *Developmental Cell* **28** 7–17
Man A J, Davis H E, Itoh A, Leach J K and Bannerman P 2011 Neurite outgrowth in fibrin gels is regulated by substrate stiffness *Tissue Eng.* A **17** 2931–42
Massensini A R, Ghuman H, Saldin L T, Medberry C J, Keane T J, Nicholls F J, Velankar S S, Badylak S F and Modo M 2015 Concentration-dependent rheological properties of ECM hydrogel for intracerebral delivery to a stroke cavity *Acta Biomater.* **27** 116–30
Medberry C J *et al* 2013 Hydrogels derived from central nervous system extracellular matrix *Biomaterials* **34** 1033–40
Mokarram N, Merchant A, Mukhatyar V, Patel G and Bellamkonda R V 2012 Effect of modulating macrophage phenotype on peripheral nerve repair *Biomaterials* **33** 8793–801
Myers J P, Santiago-Medina M and Gomez T M 2011 Regulation of axonal outgrowth and pathfinding by integrin–ECM interactions *Developmental Neurobiol.* **71** 901–23
Neubauer D, Graham J B and Muir D 2007 Chondroitinase treatment increases the effective length of acellular nerve grafts *Exp. Neurol.* **207** 163–70
National Spinal Cord Injury Statistics Center 2016 *Facts and Figures at a Glance* (Birmingham, AL: University of Alabama at Birmingham)
Patel V, Joseph G, Patel A, Patel S, Bustin D, Mawson D, Tuesta L M, Puentes R, Ghosh M and Pearse D D 2010 Suspension matrices for improved Schwann-cell survival after implantation into the injured rat spinal cord *J. Neurotrauma* **27** 789–801
Prest T A, Yeager E, LoPresti S T, Zygelyte E, Martin M J, Dong L, Gibson A, Olutoye O O, Brown B N and Cheetham J 2017

Nerve-specific, xenogeneic extracellular matrix hydrogel promotes recovery following peripheral nerve injury *J. Biomed. Mater. Res.* A **106** 450–9

Roosens A, Somers P, De Somer F, Carriel V, Van Nooten G and Cornelissen R 2016 Impact of detergent-based decellularization methods on porcine tissues for heart valve engineering *Ann. Biomed. Eng.* **44** 2827–39

Sachdeva R, Theisen C C, Ninan V, Twiss J L and Houlé J D 2016 Exercise dependent increase in axon regeneration into peripheral nerve grafts by propriospinal but not sensory neurons after spinal cord injury is associated with modulation of regeneration-associated genes *Exp. Neurol.* **276** 72–82

Sandrow-Feinberg H R, Izzi J, Shumsky J S, Zhukareva V and Houle J D 2009 Forced exercise as a rehabilitation strategy after unilateral cervical spinal cord contusion injury *J. Neurotrauma* **26** 721–31

Seidlits S K, Khaing Z Z, Petersen R R, Nickels J D, Vanscoy J E, Shear J B and Schmidt C E 2010 The effects of hyaluronic acid hydrogels with tunable mechanical properties on neural progenitor cell differentiation *Biomaterials* **31** 3930–40

Seif-Naraghi S B, Horn D, Schup-Magoffin P J and Christman K L 2012 Injectable extracellular matrix derived hydrogel provides a platform for enhanced retention and delivery of a heparin-binding growth factor *Acta Biomater.* **8** 3695–703

Seif-Naraghi S B, Salvatore M A, Schup-Magoffin P J, Hu D P and Christman K L 2010 Design and characterization of an injectable pericardial matrix gel: a potentially autologous scaffold for cardiac tissue engineering *Tissue Eng.* A **16** 2017–27

Sicari B M, Dziki J L, Siu B F, Medberry C J, Dearth C L and Badylak S F 2014 The promotion of a constructive macrophage phenotype by solubilized extracellular matrix *Biomaterials* **35** 8605–12

Tajdaran K, Gordon T, Wood M D, Shoichet M S and Borschel G H 2016 A glial cell line-derived neurotrophic factor delivery system enhances nerve regeneration across acellular nerve allografts *Acta Biomater.* **29** 62–70

Tom V J, Sandrow-Feinberg H R, Miller K, Santi L, Connors T, Lemay M A and Houlé J D 2009 Combining peripheral nerve grafts and chondroitinase promotes functional axonal regeneration in the chronically injured spinal cord *J. Neurosci.* **29** 14881–90

Tukmachev D *et al* 2016 Injectable extracellular matrix hydrogels as scaffolds for spinal cord injury repair *Tissue Eng.* A **22** 306–17

Wang R M, Johnson T D, He J, Rong Z, Wong M, Nigam V, Behfar A, Xu Y and Christman K L 2017 Humanized mouse model for assessing the human immune response to xenogeneic and allogeneic decellularized biomaterials *Biomaterials* **129** 98–110

Williams R R, Henao M, Pearse D D and Bunge M B 2015 Permissive Schwann cell graft/spinal cord interfaces for axon regeneration *Cell Transplant.* **24** 115–31

Zuidema J M, Rivet C J, Gilbert R J and Morrison F A 2014 A protocol for rheological characterization of hydrogels for tissue engineering strategie *J. Biomed. Mater. Res.* B **102** 1063–73